COMMUNICATIONS CHEMISTRY

ARTICLE

DOI: 10.1038/s42004-017-0001-z OPEN

Generic approach to access barriers in dehydrogenation reactions

Liang Yu [1,2], Laia Vilella[1] & Frank Abild-Pedersen[2]

The introduction of linear energy correlations, which explicitly relate adsorption energies of reaction intermediates and activation energies in heterogeneous catalysis, has proven to be a key component in the computational search for new and promising catalysts. A simple linear approach to estimate activation energies still requires a significant computational effort. To simplify this process and at the same time incorporate the need for enhanced complexity of reaction intermediates, we generalize a recently proposed approach that evaluates transition state energies based entirely on bond-order conservation arguments. We show that similar variation of the local electronic structure along the reaction coordinate introduces a set of general functions that accurately defines the transition state energy and are transferable to other reactions with similar bonding nature. With such an approach, more complex reaction intermediates can be targeted with an insignificant increase in computational effort and without loss of accuracy.

[1] Department of Chemical Engineering, SUNCAT Center for Interface Science and Catalysis, Stanford University, Stanford, CA 94305, USA. [2] SUNCAT Center for Interface Science and Catalysis, SLAC National Accelerator Laboratory, 2575 Sand Hill Road, Menlo Park, CA 94025, USA. Correspondence and requests for materials should be addressed to F.A-P. (email: abild@slac.stanford.edu)

In the last decade, developments in density functional theory (DFT) methods have made it possible to effectively perform computer-based screening studies in the design of heterogeneous catalysts[1–10]. The combination of explicit DFT-calculated adsorption energies (i.e., descriptors) and simple modeling methods, which describe effectively and accurately the correlation between these descriptors and complex reaction and activation energies, is an instrumental tool in this approach. Models that are first order in energy, so-called linear scaling methods, have shown to provide sufficient accuracy when evaluating trends in catalytic activity[11]. However, recently it has been shown that the linearity is closely connected to the intrinsic bond-order of the intermediate, thus suggesting that while accurate for the energy of stable intermediates on a potential energy surface (PES), it will be less accurate in describing the energy of metastable intermediates such as transition states[12,13]. Instead we have introduced a new method, "*r*-scaling", which explicitly takes variations in bond-order along the reaction coordinate into account. This directly incorporates structural variations of transition states into the energy correlations and should potentially be more accurate than typical linear approaches, such as Brønsted–Evans–Polanyi-type relations[14–19]. In addition, it also substantially reduces the computational cost when establishing transition state (TS) energy correlations[13,20,21].

The *r*-scaling scheme is built entirely on the bond-order conservation principle, which relies on the hypothesis that any transient structure (defined by the reaction coordinate *r*) between the initial and final state of an elementary reaction step along the minimum energy reaction pathway obey the following linear relation:

$$E^{\mathrm{t}}\left(r, E^{\mathrm{d}}\right) = \gamma(r)E^{\mathrm{d}} + \xi(r), \qquad (1)$$

where E^{t} (r, E^{d}) and E^{d} are the chemisorption energies of a transient intermediate at a specific reaction coordinate *r* and that of a reaction relevant descriptor species, respectively. The constraints imposed by this hypothesis uniquely define both $\gamma(r)$ and $\xi(r)$, and the TS energies as a function of E^{d} can be obtained by maximizing the potential energy E^{t} (r, E^{d}) given by Eq. (1) along the reaction coordinate.

According to the bond-order conservation principle, the dissociation of a covalent bond on a surface is associated with a relocation of the electrons into the new bonds established between the surface and the fragments of the adsorbate such that

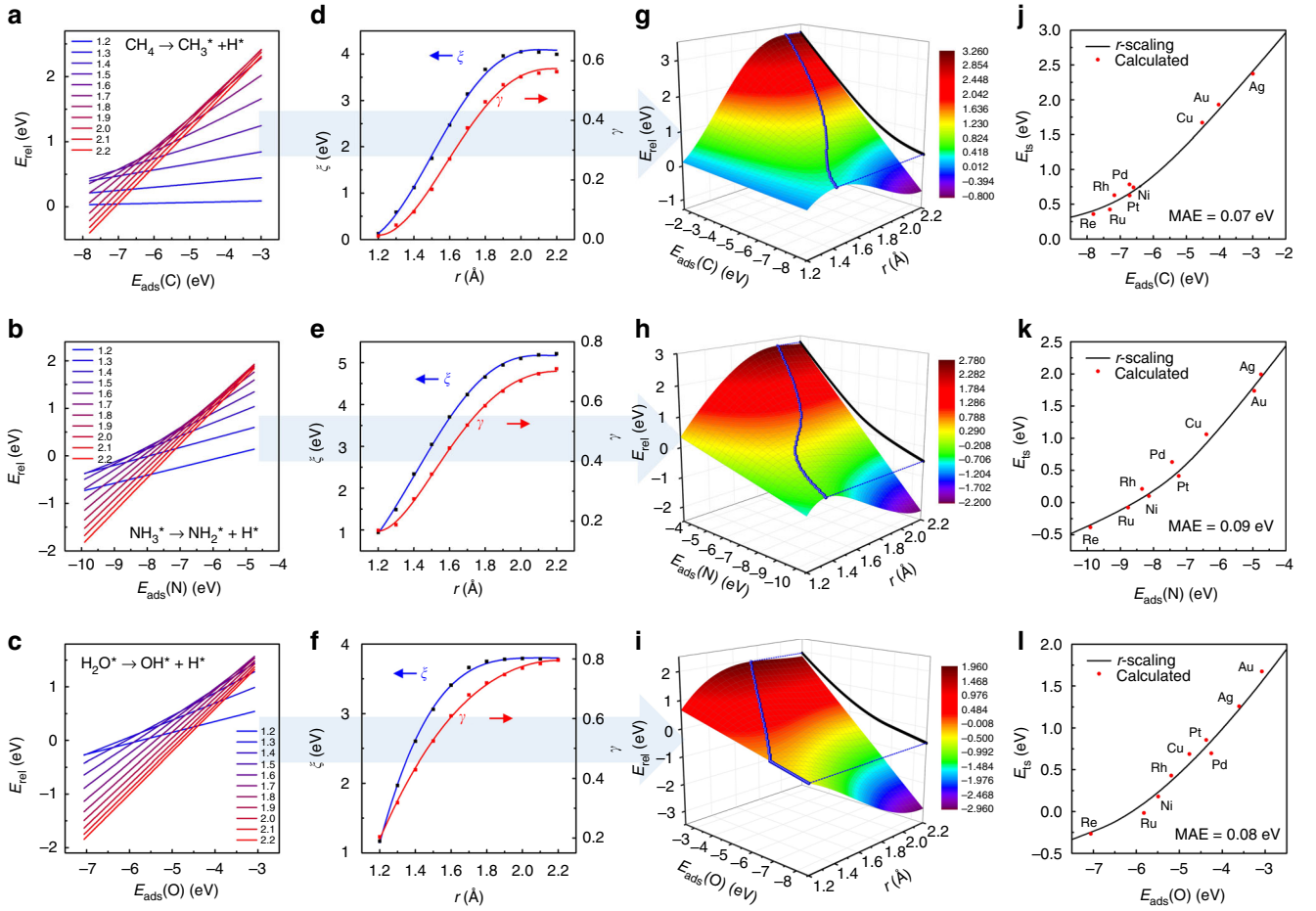

Fig. 1 Framework for the *r*-scaling scheme. **a**–**c** Linear energy-scaling relations of transient structures at fixed bond lengths *r* ranging from 1.2 to 2.2 Å for CH_4, NH_3*, and H_2O* activation on nine transition-metal (211) surfaces, respectively. The fits are obtained from linear regression of the calculated points (Supplementary Figures 1–3). Here we define $E^{\mathrm{d}} = E_{\mathrm{ads}}(\mathrm{A})_{\mathrm{A=C,N,O}} = \mathrm{E_{A@surf}} - \mathrm{E_{surf}} - \mathrm{E_{A(g)}}$ and $E^{\mathrm{t}} = E_{\mathrm{rel}}(\mathrm{AH}_{x-1}{-}\mathrm{H})_{\mathrm{A=C,N,O}} = E_{\mathrm{AH}_{x-1}-\mathrm{H@surf}} - E_{\mathrm{surf}} - E_{\mathrm{AH}_x(\mathrm{g})}$, where $E_{\mathrm{A@surf}}$ and $E_{\mathrm{AH}_x-\mathrm{H@surf}}$ are the total energies of the adsorbed surface structures. E_{surf} is the total energy of the surface, $E_{\mathrm{A(g)}}$ the gas-phase energies of C, N, and O, and $E_{\mathrm{AH}_x(\mathrm{g})}$ the gas-phase energy of CH_4, NH_3, and H_2O. The parameter *x* has the value 4, 3, and 2 for C, N, and O, respectively. **d**–**f** Fitted curves of slope γ and intercept ξ for the lines in **a**–**c** as functions of *r* (see Methods, and Supplementary Table 1). **g**–**i** PESs for CH_4, NH_3*, and H_2O* activation, respectively. **j**–**l** The TS energy-scaling relations as obtained from the *r*-scaling scheme together with explicit DFT-calculated energies for CH_4, NH_3*, and H_2O* activation, respectively. All the TS structures are shown in the Supplementary Figures 4–6

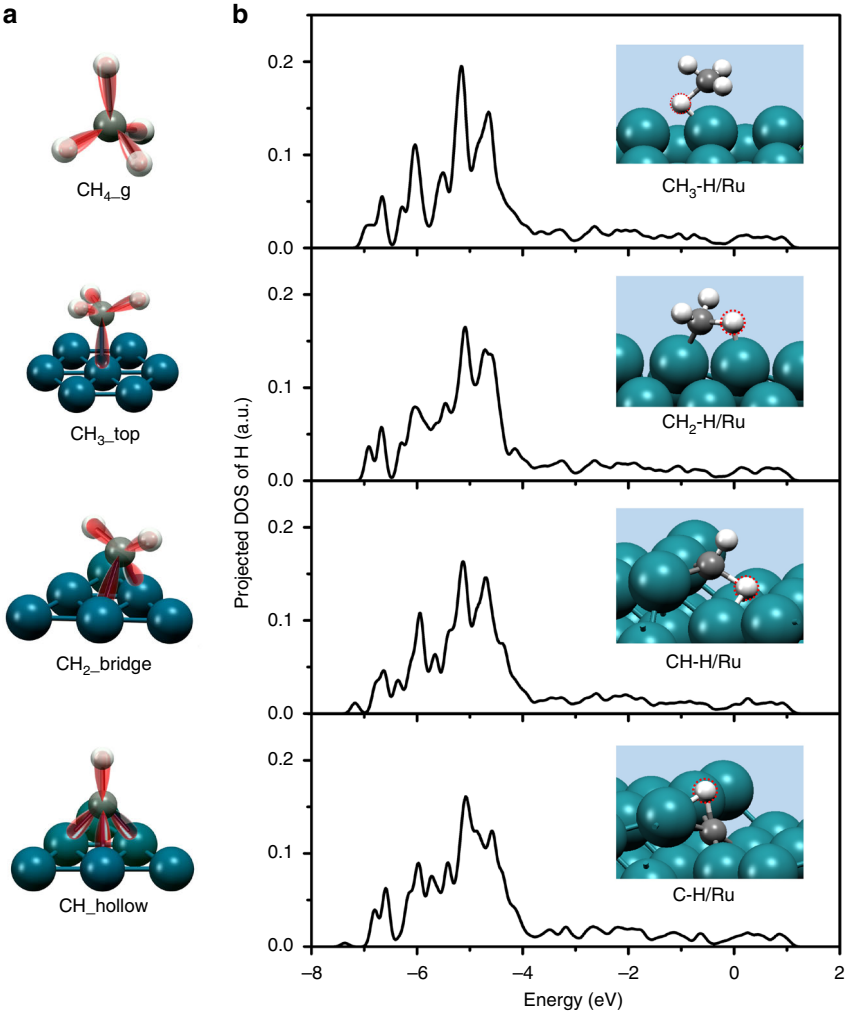

Fig. 2 Bonding features and electronic state analysis of C_1 species. **a** sp^3-hybridized bonding feature of CH_4 in the gas phase, CH_3 adsorbed on the top site, CH_2 on the bridge site and CH on the hollow site. **b** Projected density of states (PDOS) of the H atom in the transient structures of CH_3–H, CH_2–H, CH–H, and C–H on Ru(211) surface with r fixed at 1.5 Å

the normalized bond order of the fragments is conserved[22–26]. The electronic details of this process are characterized by the distinct type of bond that is broken and the associated functional forms of $\gamma(r)$ and $\xi(r)$ in Eq. (1), related to the specific orbitals in the bond and their interaction with the surface. This suggests that the cleavage of chemical bonds exhibiting the same local electronic environment can be grouped into classes. The members in each class expose a similar electron redistribution, and therefore, will share the same functional form of $\gamma(r)$ and $\xi(r)$.

In this work, we will justify this concept and demonstrate that the functions $\gamma(r)$ and $\xi(r)$, as defined in Eq. (1), are transferable between reactions within the same class. This allows us to obtain the TS energy-scaling relations for a large number of reactions from a database of template functions of $\gamma(r)$ and $\xi(r)$ determined accurately for a single element in the class. The functional form for all elements within the class can be easily generated by rescaling the template functions, which requires fewer calculations than establishing the functions for each individual reaction. In the following, we use the dehydrogenation reactions of sp^3 hybridized C, N, and O atoms to apply this concept. We show explicitly that when using the functions $\gamma(r)$ and $\xi(r)$ derived from CH_4, NH_3*, and H_2O* bond activation as our template functions to define each class, we can effectively and accurately derive the TS energy-scaling relations of any other sp^3-hybridized C–H, N–H, and O–H dissociation reaction. This not only broadens our understanding of chemical reactions and how the reaction energy evolves, it also significantly speeds up our computational approach.

Results

Application of *r*-scaling to dehydrogenation reactions. We have studied dehydrogenation reactions of hydrocarbons, ammonia, amine, water, and alcohols, which all contain sp^3-hybridized bonds, to illustrate the underlying similarity between specific bond-breaking reactions and how this can be used to address a larger set of reactions at little extra computational cost. The reaction steps examined are listed below. By considering the activation of CH_4, NH_3*, and H_2O* molecules on fcc(211) surfaces as representatives for dehydrogenation reactions of species containing C, N, and O centers, we applied the r-scaling scheme to derive the functional form of $\gamma(r)$ and $\xi(r)$ for each reaction and identify transient intermediate energies as a function of r and E^d through Eq. (1), as shown in Fig. 1.

$$CH_4^* + {}^* \rightarrow CH_3^* + H^* \quad (2)$$

$$CH_3^* + {}^* \rightarrow CH_2^* + H^* \quad (3)$$

$$CH_2^* + {}^* \rightarrow CH^* + H^* \quad (4)$$

$$CH^* + * \rightarrow C^* + H^* \quad (5)$$

$$CH_3CH_2^* + * \rightarrow CH_3CH^* + H^* \quad (6)$$

$$CH_3CH_2CH_2^* + * \rightarrow CH_3CH_2CH^* + H^* \quad (7)$$

$$NH_3^* + * \rightarrow NH_2^* + H^* \quad (8)$$

$$NH_2^* + * \rightarrow NH^* + H^* \quad (9)$$

$$NH^* + * \rightarrow N^* + H^* \quad (10)$$

$$CH_3NH^* + * \rightarrow CH_3N^* + H^* \quad (11)$$

$$H_2O^* + * \rightarrow OH^* + H^* \quad (12)$$

$$OH^* + * \rightarrow O^* + H^* \quad (13)$$

$$CH_3OH^* + * \rightarrow CH_3O^* + H^* \quad (14)$$

$$C_2H_5OH^* + * \rightarrow C_2H_5O^* + H^* \quad (15)$$

$$C_3H_7OH^* + * \rightarrow C_3H_7O^* + H^* \quad (16)$$

For all transient structures with fixed bond lengths ranging from 1.2 to 2.2 Å, the slope and intercept of the scaling of chemisorption energies (i.e., E^t as a function of E^d) changes uniformly as the bond is splitting (Fig. 1a–c). The observed increase in the slope stems from the bond-order conservation and is a manifestation of the increasing surface-adsorbate bond order as the R–H bond is breaking[20,21]. The surface corresponding to $E^d = 0$ in Fig. 1g–i identifies the intercept ξ, which can be interpreted as the potential energy of the reaction proceeding on a non-interacting surface. On the basis of the linear relations in Eq. (1), the monotonically increasing functions $\gamma(r)$ and $\xi(r)$ can be fitted as shown in Fig. 1d–f and the 2D PES for the three reactions shown in Fig. 1g–i can be derived from Eq. (1). The first order saddle points on the 2D PES (blue lines) define the TS energies, which are obtained by maximizing Eq. (1) along the reaction coordinate r:

$$E_{ts}(E_{ads}(A))_{A=C,N,O} = \max_r[\gamma(r)E_{ads}(A) + \xi(r)]. \quad (17)$$

Equation (17) defines the mapping of these saddle-point energies into a set of functions depending only on a single descriptor $(E_{ads}(A))_{A=C,N,O}$. These functions represent the TS energy-scaling relations (solid black lines in Fig. 1g–i). When compared with the actual calculated TS energies, we find a mean absolute error (MAE) of 0.07, 0.09, and 0.08 eV for the activation of CH_4, NH_3*, and H_2O*, respectively, as shown in Fig. 1j–l. Using the r-scaling scheme, TS scaling relations of all the dehydrogenation reactions can be derived as shown in Supplementary Figure 7.

The $\gamma(r)$ function in Eq. (1) reflects the intrinsic variation in the bond-order between the surface and the reactant and therefore, it changes independently of the orientation of the catalyst surface. In contrast, the function $\xi(r)$ in Eq. (1) has a very strong dependence on the surface orientation, and therefore needs to be determined specifically for a certain reaction coordinate. However, when bond-breaking processes involve a specific bonding network along a well-defined reaction coordinate, such as sp^3-hybridized bonds (e.g., CH_4, *CH_3, *CH_2, and *CH), these processes will form a class of reactions where all members share similar functional forms of $\gamma(r)$ and $\xi(r)$. As a result, each reaction in the class will experience similar electron redistribution along the reaction coordinate as reflected in the comparison of molecular orbital and projected densities of states for C_1 dehydrogenation reactions shown in Fig. 2a and b. In the following, we justify that through a simple rescaling, the functions $\gamma(r)$ and $\xi(r)$ can be transferred between bond dissociation reactions belonging to the same class. The corresponding PES can then be found through Eq. (1) and the TS energies can be derived from Eq. (17).

Once the members of a specific class have been identified, a successful rescaling of the functions $\gamma(r)$ and $\xi(r)$ within the class depends on only two conditions: (1) that the template functions $\gamma_i(r)$ and $\xi_i(r)$ derived explicitly for a single element i in the class are accurately established and (2) that the initial and final values of the functions for other members $j \neq i$ are determined. Rescaling the template functions according to the initial and final points of the jth member, allows us to generate the complete set of functions for all j, as illustrated in Fig. 3. In the following, we show how the transfer scheme can be applied to a class of reactions involving C–H bond splitting. The activation of CH_4 is used to establish the set of template functions $\gamma(r)$ and $\xi(r)$ from which new functions are generated to describe the activation of CH_3*, CH_2*, and CH*. The domain for any set of the continuous functions $\gamma(r)$ and $\xi(r)$ is reduced to a generalized reaction coordinate involving only the bond distance, which in this work ranges from 1.2 to 2.2 Å. The functional values at r = 1.2 and 2.2 Å will be obtained from the linear relations described by Eq. (1) using only two metal surfaces as shown in Fig. 4a and b. The two metals are chosen, based on the established scaling relations for the equilibrium initial and final state structures of the elementary reaction step, such that the smallest energy-averaged root-mean-square error (σ_{avg}) is achieved (see Methods)[21]. For CH_3*, CH_2*, and CH* activation, the two metals with the smallest σ_{avg} are {Ag,

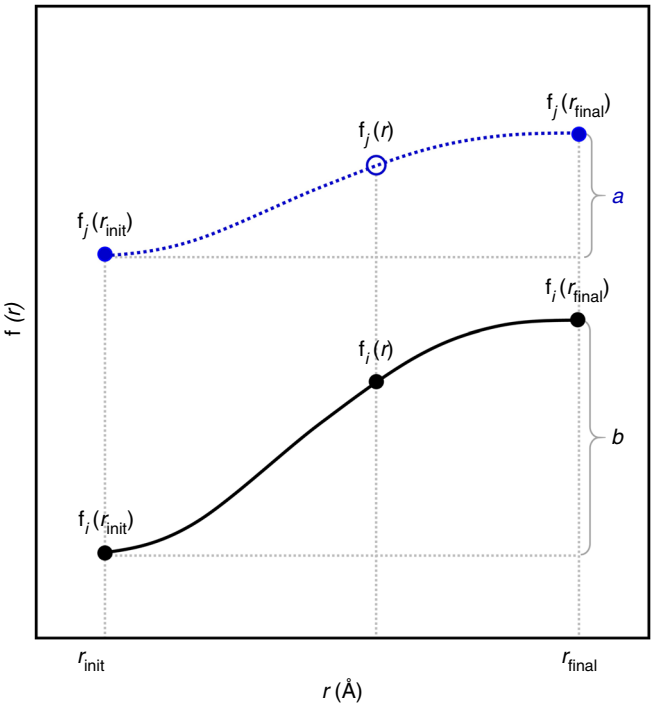

Fig. 3 Functional rescaling according to shifted initial and final state values. Objective function $f_j(r)$ is generated from rescaling template function $f_i(r)$ by $f_j(r) = f_j(r_{init}) + (a \times [f_i(r) - f_i(r_{init})])/b$, in which $a = f_j(r_{final}) - f_j(r_{init})$ and $b = f_i(r_{final}) - f_i(r_{init})$

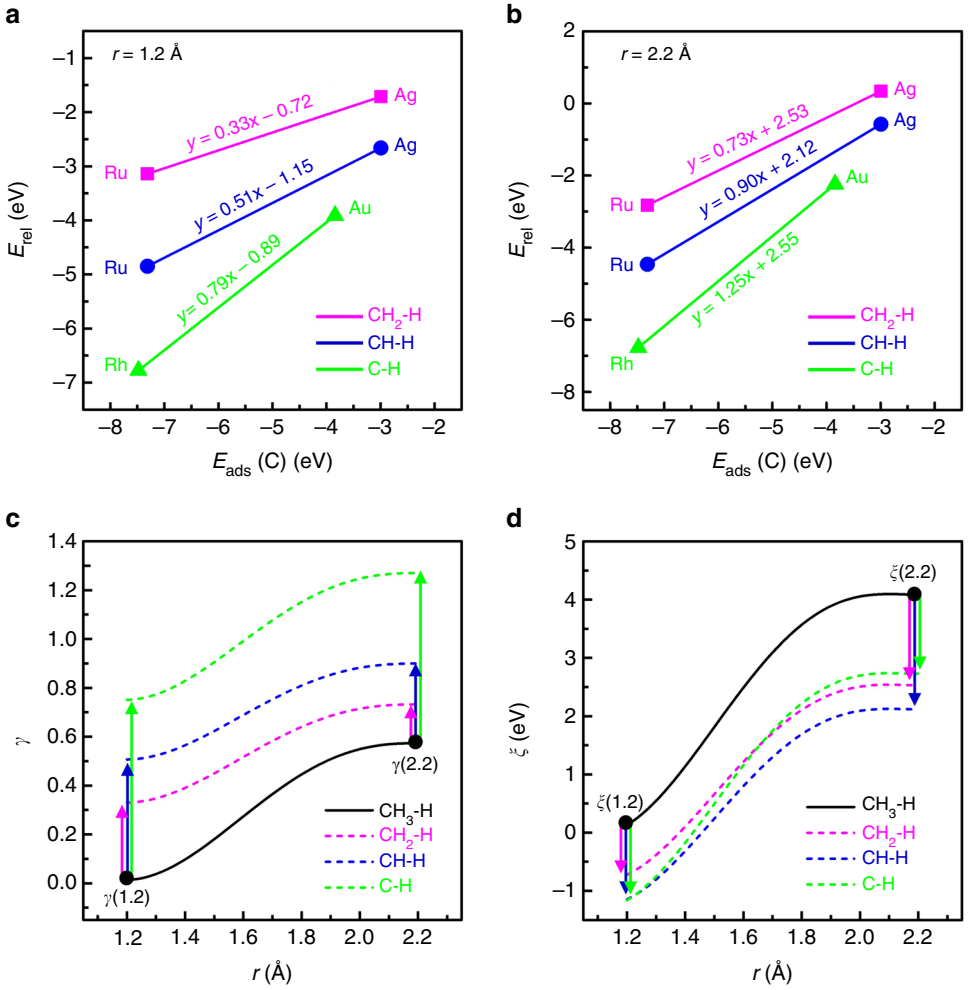

Fig. 4 Determination of the initial and final values of $\gamma(r)$ and $\xi(r)$ functions and transfer of $\gamma(r)$ and $\xi(r)$ functions. **a**, **b** The scaling relations for transient structures in the CH_3*, CH_2*, and CH* activation on (211) surfaces with bond lengths fixed at $r = 1.2$ and 2.2 Å, which are established using the selected two metal surfaces. E_{ads} of C* on the threefold hollow site is used as the descriptor for CH_4, CH_3*, and CH_2* activation. As CH* prefers the fourfold hollow site, considering the implicit adsorption behavior of carbon species on the fourfold site in which the E_{ads} is non-linearly related to that on the three(or less)-fold site[11], the E_{ads} of C* on the fourfold hollow site is used as the descriptor for CH* activation to achieve a better accuracy. **c**, **d** The transfer of $\gamma(r)$ and $\xi(r)$ functions of CH_4 activation to CH_3*, CH_2*, and CH* activation according to the slope and intercept values at $r = 1.2$ and 2.2 Å as obtained in **a**, **b**, e.g., for CH_3* activation, $\gamma(1.2) = 0.33$, $\xi(1.2) = -0.72$, $\gamma(2.2) = 0.73$, $\xi(2.2) = 2.52$

Ru}, {Ag,Ru}, and {Au,Rh}, respectively. Figure 4a and b shows the relations for CH_3*, CH_2*, and CH* as established using the two metal surfaces for C–H bond lengths fixed at $r = 1.2$ and 2.2 Å, respectively. The obtained values for slopes γ and intercepts ξ are seen to be very close to those obtained from linear relations fitted using all nine metal surfaces (Table 1) and these values are used as rescaling parameters to perform the transfer process as shown in Fig. 4c and d. TS energies for CH_3*, CH_2*, and CH* activation can now be obtained using Eq. (17). The whole process is detailed in the Methods section.

Discussion

The general scheme and the electronic structure similarities of the bonds formed between the catalyst surface and the reactants allow us to expand upon the three reaction classes defined by the functions obtained from CH_4, NH_3*, and H_2O* activation. In principle, all reactants R–H, where R is any residue forming an sp^3-hybridized bond with hydrogen through C, N, or O should fall in one of the three classes defined above, e.g., activation of CH_3*, CH_2*, CH*, CH_3CH_2*, and $CH_3CH_2CH_2$* belong to the same class as CH_4 activation, NH_2*, NH*, and CH_3NH* to the same class as NH_3* activation, and OH*, CH_3OH*, C_2H_5OH*, and C_3H_7OH* to the same class as H_2O* activation. Using the transfer scheme, we established the $\gamma(r)$ and $\xi(r)$ functions for all the members of each class and subsequently extrapolated the TS energy-scaling relations of all the considered dehydrogenation reactions from Eq. (17) (Supplementary Figure 8). In Fig. 5, a comparison is shown between the transition state energies obtained using this simple model and the energies obtained using a constrained optimization in DFT based on either the fixed bond-length method or the Nudged–Elastic–Band (NEB) approach[27,28]. Our comparison shows an overall MAE of only 0.12 eV using CH_4, NH_3*, and H_2O* activation on (211) surfaces to obtain the template functions for each class. Using alternative members to establish the template functions, the overall MAE ranges from 0.11 to 0.17 eV. It is noteworthy to mention that our model provides a much cheaper route for obtaining TS energies, since only four constrained calculations are required to secure the necessary information for a specific reaction belonging to a class with pre-established template $\gamma(r)$ and $\xi(r)$ functions. In contrast to traditional NEB methods, where TS energies are computed for every reaction step and catalyst surface, our model classifies reactions and applies a transfer scheme to effortlessly derive the

Table 1 γ and ξ values derived using two or all nine metal surfaces

Reactions	r (Å)	Using two metal surfaces		Using all nine metal surfaces	
		γ	ξ (eV)	γ	ξ (eV)
CH_3* activation	1.2	0.33	−0.72	0.32	−0.68
	2.2	0.73	2.53	0.74	2.49
CH_2* activation	1.2	0.51	−1.15	0.51	−1.17
	2.2	0.90	2.12	0.94	2.40
CH* activation	1.2	0.79	−0.89	0.76	−1.10
	2.2	1.25	2.55	1.25	2.51

TS energies thus significantly reducing the associated computational cost.

In summary, the functions $\gamma(r)$ and $\xi(r)$ are shown to depend only on the electronic nature of the activated bonds irrespective of the surface type or residual groups. Using three series of dehydrogenation reactions involving *sp*-hybridized C, N, and O on three low index metal surfaces: (100), (111), and (211), we have shown that the derived functions $\gamma(r)$ and $\xi(r)$ define three unique classes of reactions and that they can be transferred easily between bond-breaking reactions belonging to the same class. Only four constrained calculations are required to apply the transfer scheme for a given reaction step, allowing access to the full PES from which TS energies along the reaction coordinate can be derived. Moving forward, this enables us to build databases of bond specific $\gamma(r)$ and $\xi(r)$ functions for a well-defined set of surface reaction classes and then employ the transfer scheme to obtain relevant kinetic parameters. This approach introduces a significant reduction in the computational cost of calculating transition state energies. A simple estimation shows a factor of ~36 in the reduction of cpu time compared to traditional NEB methods, resulting in significant savings in power consumption as well as time spent by scientific personnel (Methods). This expansion of scaling methods to include the description of reaction transients increases the efficiency in the computation of kinetic parameters without loss of accuracy and primarily it enables an even faster screening of catalyst materials.

Methods

DFT calculations. DFT calculations are performed using the plane-wave-based PWSCF (Quantum-ESPRESSO) code and the Atomic Simulation Environment (ASE)[29]. The ultrasoft Vanderbilt pseudopotential method with BEEF exchange-correlation functional is adopted[30–33]. A cutoff energy of 500 eV for the wave-functions is used. The fcc(211), fcc(111), and fcc(100) surfaces of nine transition metals including Cu, Ni, Ag, Pd, Re, Rh, Ru, Pt, and Au are chosen as catalysts for the dehydrogenation reactions. The (211) slabs are built with 4 atomic layers in the [111] direction in rectangular 1 × 3 supercells with the bottom three [111] layers fixed during structural optimizations. The (111) and (100) slabs are built with four atomic layers with the bottom two layers fixed during structural optimizations using hexagonal 3 × 3 and rectangular 2 × 2 supercells, respectively. The Monkhorst–Pack scheme is used for sampling the Brillouin zone[34] and *k*-point grids of 4 × 2 × 1, 4 × 4 × 1 and 4 × 4 × 1 are selected for (211), (111), and (100) slabs, respectively. The vacuum thickness is set to more than 10 Å in all slab calculations and the dipole correction is applied to decouple the interaction between slabs. During structural relaxations, the residual force between atoms is converged to a value below 0.02 eV/Å.

TS energies for the dehydrogenation reactions are calculated using the fixed bond-length (FBL) method as implemented in ASE. All TS structures show a single imaginary frequency thus identifying it as a first order saddle-point. The fixed bond-length calculations range from 1.2 to 2.2 Å with increments of 0.1 Å, which is accurate enough to cover transition states of any dehydrogenation reaction. TS's with a bond-length shorter than 1.2 Å are close to the initial state, and in these cases the reaction is treated as if it has no barrier. TS energy calculations for all reactions (2–16) are performed on fcc(211) surfaces and for reactions (3), (6), and (7) calculations have also been performed on fcc(111) and fcc (100) surfaces.

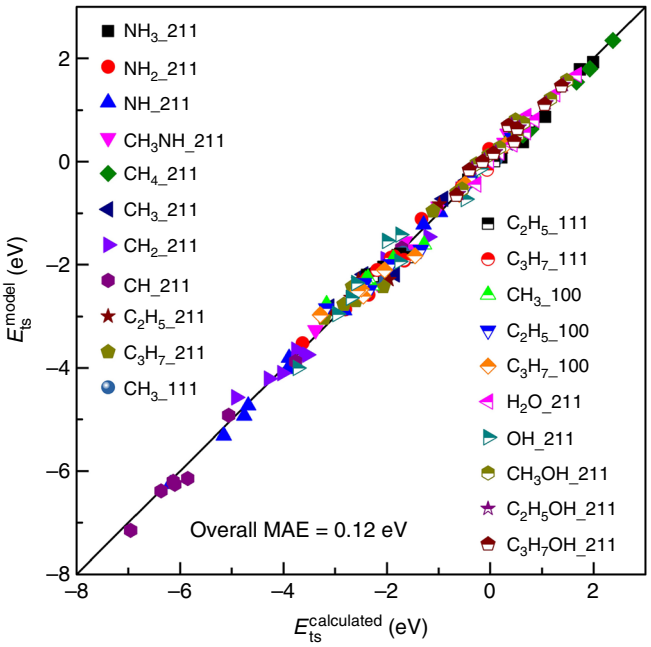

Fig. 5 The accuracy of our transfer model. Calculated TS energies are compared with the predictions from our model based on the transfer of template $\gamma(r)$ and $\xi(r)$ functions for classes of dehydrogenation reactions involving species with sp^3-hybridized C–H, N–H, or O–H bonds. The $\gamma(r)$ and $\xi(r)$ functions of CH_4, NH_3*, and H_2O* activation on fcc(211) surfaces are used as the templates for each class, respectively. Data of TS energy calculations are shown in the Supplementary Tables 2–22

Fitting procedure. In the *r*-scaling scheme, fitting of the slope $\gamma(r)$ and the intercept $\xi(r)$ is done applying the scipy.optmize.minimize method using a fifth-order polynomial. The functions are constrained to be monotonically increasing.

$$\gamma(r) = a_0 + a_1 r + a_2 r^2 + a_3 r^3 + a_4 r^4 + a_5 r^5, \quad (18)$$

$$\xi(r) = b_0 + b_1 r + b_2 r^2 + b_3 r^3 + b_4 r^4 + b_5 r^5. \quad (19)$$

Choosing the two metal surfaces. Established linear scaling relations for the initial and final state equilibrium structures for a given reaction have been used for selecting the two transition-metal surfaces. Selection of a metal surface is partly determined by the root-mean square error (σ) of the linear regressions of the initial and final state:

$$\sigma = \sqrt{(R_{IS}^2 + R_{FS}^2)/2}, \quad (20)$$

where R_{IS} and R_{FS} are the metal-specific absolute residuals of the initial and final state linear regression, respectively. The energy span of the descriptor is also a significant factor. To ensure that the metals chosen reflect both the reactive as well as the noble surfaces, we define an energy-averaged root-mean square error of two metals (m_1 and m_2) as:

$$\sigma_{avg} = \frac{\sigma_{m_1} + \sigma_{m_2}}{|E_{ads}^{m_2}(A) - E_{ads}^{m_1}(A)|}. \quad (21)$$

The choice of two transition-metal surfaces that minimizes Eq. (21) is finally used for building the scaling relations of transient structures with bond-length fixed at r = 1.2 and 2.2 Å. More details about the method selecting the two metals can be found in ref. [21].

Steps of transfer scheme for obtaining TS energy relations.

(1) Obtain the $\gamma(r)$ and $\xi(r)$ functions for a single reaction in a class using a global or simplified *r*-scaling scheme[21]. These functions will be used as the template functions for the reaction class.

(2) For a given reaction in the class, calculate adsorption energies (E_{rel}) of the initial state and final state on a sufficiently large number of metal surfaces and build the linear relations of E_{rel} vs. descriptor for the two states, from which two metal surfaces are determined as detailed above. Note that the initial and final state structures in this step are the equilibrium structures, not

those with bond-length fixed at 1.2 and 2.2 Å.
(3) Calculate the adsorption energies (E_{rel}) on the two metal surfaces determined in step (2) of two transient structures with bond-length fixed at 1.2 and 2.2 Å, respectively (four calculations total disregarding the clean surfaces and gas-phase calculations). Then build the linear relations of E_{rel} vs. descriptor for the two transient structures using just two points for each (Fig. 4a, b) and obtain the values of $\gamma(1.2)$, $\xi(1.2)$, $\gamma(2.2)$, and $\xi(2.2)$ from the linear relations.
(4) Rescale the template functions $\gamma(r)$ and $\xi(r)$ functions as shown in Fig. 3.
(5) Build the TS energy-scaling relation for the reaction according to Eq. (17).

NEB versus *r*-scaling comparison. To establish the transition state scaling relation for a specific reaction using nine catalyst surfaces, the NEB method requires:

$$8\,\text{images (per NEB)} \times 9\,\text{surfaces} \times N_{\text{core}} = 72\,N_{\text{core}}. \quad (22)$$

The *r*-scaling method needs:

$$2\,\text{images} \times 2\,\text{surfaces} \times N_{\text{core}} = 4\,N_{\text{core}}, \quad (23)$$

where N_{core} is the number of cpu-cores used per image or structure. Considering that NEB calculations take longer time to converge, we shall assume that NEB calculations take a factor of two more time than the constrained minimization calculations used in the *r*-scaling method. The difference in the number of cores used is $(2{\times}72N_{core})/4N_{core} = 36$, in favor of *r*-scaling. Thus *r*-scaling introduces a substantial reduction in cpu time, which renders it a highly efficient and accurate method for estimating TS energies.

Data availability. Part of the data sets generated and analysed during the current study are included in the Supplementary Information file and others are available in the "figshare" repository, https://doi.org/10.6084/m9.figshare.5601622.v2.

Received: 25 September 2017 Accepted: 22 November 2017
Published online: 08 March 2018

References

1. Honkala, K. et al. Ammonia synthesis from first-principles calculations. *Science* **307**, 555–558 (2005).
2. Van Santen, R. A. & Neurock, M. Concepts in theoretical heterogeneous catalytic reactivity. *Catal. Rev. Sci. Eng.* **37**, 557–698 (1995).
3. Norskov, J. K., Bligaard, T., Rossmeisl, J. & Christensen, C. H. Towards the computational design of solid catalysts. *Nat. Chem.* **1**, 37–46 (2009).
4. Greeley, J., Jaramillo, T. F., Bonde, J., Chorkendorff, I. & Norskov, J. K. Computational high-throughput screening of electrocatalytic materials for hydrogen evolution. *Nat. Mater.* **5**, 909–913 (2006).
5. Greeley, J. & Mavrikakis, M. Alloy catalysts designed from first principles. *Nat. Mater.* **3**, 810–815 (2004).
6. Greeley, J. et al. Alloys of platinum and early transition metals as oxygen reduction electrocatalysts. *Nat. Chem.* **1**, 552–556 (2009).
7. Linic, S. & Christopher, P. Overcoming limitation in the design of selective solid catalysts by manipulating shape and size of catalytic particles: epoxidation reactions on silver. *ChemCatChem.* **2**, 1061–1063 (2010).
8. Salciccioli, M. & Vlachos, D. G. Kinetic modeling of Pt catalyzed and computation-driven catalyst discovery for ethylene glycol decomposition. *ACS Catal.* **1**, 1246–1256 (2011).
9. Mpourmpakis, G. & Vlachos, D. G. Computational-based catalyst design for thermochemical transformations. *MRS Bull.* **36**, 211–215 (2011).
10. Montemore, M. M. & Medlin, J. W. Scaling relations between adsorption energies for computational screening and design of catalysts. *Catal. Sci. Technol.* **4**, 3748–3761 (2014).
11. Abild-Pedersen, F. et al. Scaling properties of adsorption energies for hydrogen-containing molecules on transition-metal surfaces. *Phys. Rev. Lett.* **99**, 016105 (2007).
12. Calle-Vallejo, F., Loffreda, D., KoperMarc, T. M. & Sautet, P. Introducing structural sensitivity into adsorption–energy scaling relations by means of coordination numbers. *Nat. Chem.* **7**, 403–410 (2015).
13. Abild-Pedersen, F. Computational catalyst screening: scaling, bond-order and catalysis. *Catal. Today* **272**, 6–13 (2016).
14. Bell, R. P. The theory of reactions involving proton transfers. *Proc. R. Soc. Lond. A* **154**, 414–429 (1936).
15. Evans, M. G. & Polanyi, M. Inertia and driving force of chemical reactions. *Trans. Faraday Soc.* **34**, 11–24 (1938).
16. Cheng, J. et al. Brønsted–Evans–Polanyi relation of multistep reactions and volcano curve in heterogeneous catalysis. *J. Phys. Chem. C* **112**, 1308–1311 (2008).
17. Bligaard, T. et al The Brønsted–Evans–Polanyi relation and the volcano curve in heterogeneous catalysis. *J. Catal.* **224**, 206–217 (2004).
18. Wang, S. et al. Universal Brønsted–Evans–Polanyi relations for C–C, C–O, C–N, N–O, N–N, and O–O dissociation reactions. *Catal. Lett.* **141**, 370–373 (2011).
19. van Santen, R. A. & Neurock, M. Theory of surface chemical reactivity. *Russ. J. Phys. Chem. B* **1**, 261–291 (2007).
20. Plessow, P. N. & Abild-Pedersen, F. Examining the linearity of transition state scaling relations. *J. Phys. Chem. C.* **119**, 10448–10453 (2015).
21. Yu, L. & Abild-Pedersen, F. Bond order conservation strategies in catalysis applied to the NH3 decomposition reaction. *ACS Catal.* **7**, 864–871 (2017).
22. Shustorovich, E. Chemisorption phenomena: analytic modeling based on perturbation theory and bond-order conservation. *Surf. Sci. Rep.* **6**, 1–63 (1986).
23. Shustorovich, E. Heat of molecular chemisorption from bond-order-conservation viewpoint: why morse potentials are so efficient. *Surf. Sci.* **181**, L205–L213 (1987).
24. Shustorovich, E. Metal effects in the Fischer–Tropsch synthesis: bond-order-conservation-morse-potential approach. *Catal. Lett.* **7**, 107–118 (1990).
25. Shustorovich, E. & Sellers, H. The UBI-QEP method: a practical theoretical approach to understanding chemistry on transition metal surfaces. *Surf. Sci. Rep.* **31**, 1–119 (1998).
26. van Santen, R. A. On Shustorovich's bond-order conservation method as applied to chemisorption. *Recl. Trav. Chim. Pays-Bas* **109**, 59–63 (1990).
27. Henkelman, G. & Jónsson, H. Improved tangent estimate in the nudged elastic band method for finding minimum energy paths and saddle points. *J. Chem. Phys.* **113**, 9978–9985 (2000).
28. Henkelman, G., Uberuaga, B. P. & Jónsson, H. A climbing image nudged elastic band method for finding saddle points and minimum energy paths. *J. Chem. Phys.* **113**, 9901–9904 (2000).
29. Paolo, G. et al. QUANTUM ESPRESSO: a modular and open-source software project for quantum simulations of materials. *J. Phys. Condens. Matter* **21**, 395502 (2009).
30. Vanderbilt, D. Soft self-consistent pseudopotentials in a generalized eigenvalue formalism. *Phys. Rev. B* **41**, 7892–7895 (1990).
31. Laasonen, K., Pasquarello, A., Car, R., Lee, C. & Vanderbilt, D. Car–Parrinello molecular dynamics with Vanderbilt ultrasoft pseudopotentials. *Phys. Rev. B* **47**, 10142–10153 (1993).
32. Laasonen, K., Car, R., Lee, C. & Vanderbilt, D. Implementation of ultrasoft pseudopotentials in *ab initio* molecular dynamics. *Phys. Rev. B* **43**, 6796–6799 (1991).
33. Wellendorff, J. et al. Density functionals for surface science: exchange-correlation model development with Bayesian error estimation. *Phys. Rev. B* **85**, 235149 (2012).
34. Monkhorst, H. J. & Pack, J. D. Special points for Brillouin-zone integrations. *Phys. Rev. B* **13**, 5188–5192 (1976).

Acknowledgements

We acknowledge support from the U.S. Department of Energy, Office of Basic Energy Sciences, to the SUNCAT Center for Interface Science and Catalysis at SLAC National Accelerator Laboratory and Stanford University.

Author contributions

L.Y. conducted all DFT calculations for the N–H and O–H bonds dissociation reactions and processed and analyzed data. L.V. conducted all DFT calculations for C–H bond dissociation reactions. F.A.-P. conceived the calculations and analyzed results. All the authors interpreted the structures and contributed to the preparation of the manuscript.

Additional information

Supplementary information is available for this paper at https://doi.org/10.1038/s42004-017-0001-z.

Competing interests: The authors declare no competing financial interests.

Reprints and permission information is available online at http://npg.nature.com/reprintsandpermissions/

Publisher's note: Springer Nature remains neutral with regard to jurisdictional claims in published maps and institutional affiliations.